Structural and Functional Characterization of the C-Terminal Domain of the Ecdysteroid Phosphate Phosphatase from *Bombyx mori* Reveals a New Enzymatic Activity[†]

Yunting Chen,[‡] Jean Jakoncic,[§] Jin Wang,[||,⊥] Xiliang Zheng,[⊥] Nick Carpino,[¶] and Nicolas Nassar*[,‡]

Department of Physiology and Biophysics, Stony Brook University, Basic Sciences Tower, Stony Brook, New York 11794-8661, National Synchrotron Light Source, Brookhaven National Laboratory, Building 725, Upton, New York 11973, Department of Chemistry, Physics, and Applied Mathematics, Stony Brook University, Stony Brook, New York 11794-3400, Changchun Institute of Applied Chemistry, State Key Laboratory of Electroanalytical Chemistry, Chinese Academy of Sciences, Changchun, Jilin 130022, People's Republic of China, and Department of Molecular Genetics and Microbiology, Life Sciences Building, Stony Brook University, Stony Brook, New York 11794-5222

Received July 11, 2008; Revised Manuscript Received September 19, 2008

ABSTRACT: Here, we present the crystal structure of the ecdysone phosphate phosphatase (EPPase) phosphoglycerate mutase (PGM) homology domain, the first structure of a steroid phosphate phosphatase. The structure reveals an α/β-fold common to members of the two histidine (2H)-phosphatase superfamily with strong homology to the Suppressor of T-cell receptor signaling-1 (Sts-1_{PGM}) protein. The putative $EPPase_{PGM}$ active site contains signature residues shared by 2H-phosphatase enzymes, including a conserved histidine (His80) that acts as a nucleophile during catalysis. The physiological substrate ecdysone 22-phosphate was modeled in a hydrophobic cavity close to the phosphate-binding site. $EPPase_{PGM}$ shows limited substrate specificity with an ability to hydrolyze steroid phosphates, the phospho-tyrosine (pTyr) substrate analogue *para*-nitrophenylphosphate (*p*NPP) and pTyr-containing peptides and proteins. Altogether, our data demonstrate a new protein tyrosine phosphatase (PTP) activity for EPPase. They suggest that EPPase and its closest homologues can be grouped into a distinct subfamily in the large 2H-phosphatase superfamily of proteins.

In invertebrates, the ecdysteroid hormones (ecdysone and its derivatives) regulate the major stages of development including growth, body size, cellular division, programmed cell death, color change, molting, and metamorphosis (*1*−*6*). They do so by binding to the ecdysone receptor (EcR),[1] a ligand-inducible transcription factor that controls the expression of genes involved in ecdysis and metamorphosis. The important roles of various ecdysteroid hormones for embryonic development in insects have been well demonstrated in the eggs of the silkworm *Bombyx mori* and the fly *Drosophila* (*7*). Ecdysone, the prohormone of the major insect molting hormone 20-hydroxyecdysone (20E), is synthesized from cholesterol and controls the timing of molting (*8*). In particular, analysis of the interaction between the ecdysteroid receptor and various egg ecdysteroids of *B. mori* suggested that 20E is responsible for the development difference between diapause and nondiapause in *B. mori* embryos (*9*). Additionally, recent findings revealed a coordinated cross talk between the ecdysone and insulin signaling pathways to regulate growth and developmental timing to determine final body size (*10*−*12*).

In insects, ecdysteroid hormones undergo inactivation by phosphorylation and are stored as physiologically inactive hormones until needed. Recently, an ecdysteroid phosphate phosphatase (EPPase) was identified from *B. mori* eggs with specificity for ecdysteroid phosphates that have a phosphate group at position 22 on the side chain of the steroid. EPPase converts inactive ecdysteroid phosphate, ecdysone 22-phosphate (E22P) and 20-hydroxyecdysone 22-phosphate (20E22P), to active phosphate-free ecdysteroids (Scheme 1), including 20E, in *B. mori* eggs (*9*) and is therefore essential for the proper signaling of 20E. EPPase is expressed in nondiapause but not in diapause eggs and its expression pattern correlates with the amount of free ecdysteroids in nondiapause eggs. The full-length cDNA of EPPase was isolated by reverse transcription polymerase chain reaction

[†] Research in N.N.'s laboratory is supported in part by grants from the NIH (No. CA-115611) and DOD (No. NF060060). Research in N.C.'s laboratory is supported by grants from The Arthritis Foundation (No. LI07), NIH-NIAID (No. R21AI075176), and The National Multiple Sclerosis Society through a Collaborative MS Research Center Award (No. CA1044A1). Research carried out at X6A beam line, National Synchrotron Light Source, Brookhaven National Laboratory, is supported by the U.S. Department of Energy under Contract No. DE-AC02-98CH10886. X6A is funded by NIH/NIGMS under agreement Y1 GM-0080-03.

* To whom correspondence should be addressed. Tel: 631-444-3521. Fax: 631-444-3432. E-mail: nicolas.nassar@sunysb.edu.

[‡] Department of Physiology and Biophysics, Stony Brook University.

[§] Brookhaven National Laboratory.

[||] Department of Chemistry, Physics, and Applied Mathematics, Stony Brook University.

[⊥] Chinese Academy of Sciences.

[¶] Department of Molecular Genetics and Microbiology, Stony Brook University.

[1] Abbreviations: DTT, dithiothreitol; EcR, ecdysone receptor; EPPase, ecdysteroid phosphate phosphatase; PGM, phosphoglycerate mutase; *p*NP, *para*-nitrophenol; *p*NPP, *para*-nitrophenylphosphaste; PTP, protein tyrosine phosphatase; Sts, suppressor of T cell signaling; pTyr, phosphotyrosine.

10.1021/bi801318w CCC: $40.75
Published on Web 10/21/2008

Scheme 1: Activation of Ecdysone 22-Phosphate by EPPase

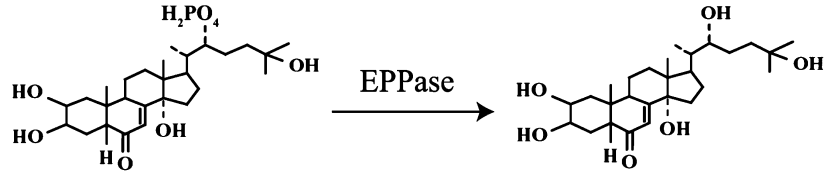

Ecdysone 22-phosphate Ecdysone

using the partial amino acid sequence obtained from purified EPPase from nondiapause *B. mori* eggs (*9*). The cloned protein consists of a single recognizable domain of 331 amino acids that contains the signature sequence ^{79}RHGE^{82} common to members of the 2H-phosphatase superfamily of enzymes also known as the PGM superfamily (*13, 14*). Recently, a sequence search of the database resulted in the cloning of a longer EPPase isoform from *Drosophila* that contains a ubiquitin association (UBA) and a src-homology 3 (SH3) domain N-terminal to the PGM domain (*15*).

The 2H-phosphatase superfamily contains a large number of enzymes including the diverse acid phosphatases (AcPs), the cofactor dependent phosphoglycerate mutase (dPGM), fructose 2,6-bisphosphatase (F2,6BP), the bacterial phosphatase SixA, Sts-1, and many others. The substrates of these enzymes range from phosphorylated small molecules to large phosphoproteins. For example, the sensor kinase for the anaerobic respiratory control (Arc) response in *Escherichia coli* is a SixA substrate (*16*), while mammalian Sts-1 was recently shown to be the prototype of a new family of histidine-based phosphatases that appear to suppress the T cell receptor (TCR) signaling by dephosphorylating several tyrosine-phosphorylated proteins including ZAP-70 (*17*). The 2H-phosphatase superfamily has been so named because the majority of its members are phosphatases that contain two conserved histidine residues within the active site that are essential for catalysis. Some family members are also phosphotransferases (*13*). In addition to the two conserved histidines, two arginines important for catalysis are also conserved. Aside from these four residues, family members bear little primary sequence homology to one another. According to the accepted mechanism, the histidine within the RHGE signature motif is responsible for the nucleophilic attack on the substrate and becomes transiently phosphorylated. The phosphorylated histidine intermediate is then hydrolyzed, and the enzyme is ready for a new catalytic cycle. The conserved arginine residues are believed to stabilize the transition state structures that appear during the dephosphorylation reaction (*13, 14*).

In this study, we present the crystal structure of *B. mori* EPPase$_{PGM}$ and demonstrate its similarity to the recently solved structure of mammalian Sts-1$_{PGM}$. We also demonstrate and characterize a previously undescribed PTP activity of EPPase$_{PGM}$ *in vitro*. These results suggest novel functions for the invertebrate ecdysteroid phosphate phosphatase.

EXPERIMENTAL PROCEDURES

Protein Preparation. An expressed sequence tag (EST) encoding *Bombyx mori* EPPase was obtained from the database of silkworm ESTs (Silkbase) maintained by the Japanese Society for the Promotion of Science (http://morus.ab.a.u-tokyo.ac.jp/cgi-bin/index.cgi). A cDNA fragment encoding the EPPase PGM domain (residues 69−330) was amplified by PCR, sequenced to confirm absence of errors, cloned as a His-tagged protein in the pProEX-HTb vector (Life Technologies) and expressed in the *E. coli* CodonPlus BL21(DE3) strain (Stratagene) as described previously for Sts-1$_{PGM}$ (*18*). The EPPase$_{PGM}$ mutants were generated by the QuikChange XL Site-directed Mutagenesis kit (Stratagene). Proteins were purified on a Ni-NTA column (Qiagen) followed by removal of the His-tag by the action of tobacco etch virus (TEV) protease and a size exclusion column (Superdex 200, GE Healthcare).

Enzyme Activity Assays. The phosphatase activity of wild-type and mutant EPPases was measured using *p*NPP (Sigma) or various steroid phosphates (Steraloids Inc., Newport, RI) as substrate. When *p*NPP was used, the reaction mixture contained 100 mM TAB (25 mM Tris, 50 mM acetic acid, 25 mM bis-Tris), pH = 7.5, 150 mM NaCl, 0.1 mM EDTA, and 1 mM DTT. The reaction was initiated by adding the protein (50 nM) to the *p*NPP in the reaction mixture preincubated at 37 °C. The reaction was stopped by adding 13% K_2HPO_4 or 0.5 M NaOH and immediately chilled on ice. The amount of *para*-nitrophenol (*p*NP) converted from *p*NPP was quantified by measuring the absorption at 405 nm using the following relationship: $OD_{405} = \varepsilon b$[*p*NP] where $\varepsilon = 1.78 \times 10^4$ M^{-1} cm^{-1}, b = light path (cm), and [*p*NP] is the *p*NP concentration. Stock solutions (0.1 M) of prednisolone 21-phosphate disodium salt, dexamethasone 21-phosphate disodium salt, and β-methasone 21-phosphate disodium salt were prepared in water. The reaction mixture contained the same reaction buffer, but the phosphate release was measured using the malachite green assay (*19*).

k_{cat} and K_m Measurements. Initial velocities (v) were measured at various *p*NPP concentrations, [*p*NPP], as the slope of the linear part of [*p*NP] plotted as a function of time. To determine the kinetic parameters k_{cat} and K_m, v was plotted as a function of [*p*NPP] and the data points fitted to a Michaelis−Menten equation

$$v = \frac{V_{max}[p\text{NPP}]}{([p\text{NPP}] + K_m)} \quad (1)$$

using the program SigmaPlot 5.05 (SPSS Science Inc., Chicago).

Inhibition of EPPase$_{PGM}$. Tungstate, vanadate, and phosphate at various concentrations were incubated with the *p*NPP (1 mM) containing buffer at 37 °C. EPPase$_{PGM}$ (50 nM) was added to this buffer and the phosphatase activity was measured as previously described. Initial velocities (v) were plotted as a function of the inhibitor concentration, [I], and the data points were fitted with the program SigmaPlot to a competitive inhibition equation

$$v = \frac{V_{max}[p\text{NPP}]}{\{[p\text{NPP}] + K_m(1 + [\text{I}]/K_I)\}} \quad (2)$$

where K_I is the inhibition constant, [*p*NPP] = 1 mM, and K_m = 1.9 mM. The reported IC_{50} values correspond to [I] at 50% inhibition.

PTP Activity of EPPase. All assays were performed at 37 °C and pH 7.5. $EPPase_{PGM}$ (50 and 500 nM) was incubated with 1 mM pTyr-containing peptide (NH_2-SVYESP-pY-SDPEE-COOH) in 150 mM NaCl, 100 mM TAB, 0.1 mM EDTA, and 1 mM DTT in a total volume of 0.1 mL for 5 min. The reaction was stopped with 50 μL of 0.5 M NaOH, and the released inorganic phosphate was detected with the malachite green assay (*19*). Tyrosine phosphorylated proteins were obtained by anti-pTyr immunoprecipitations from TCR-stimulated murine T cells as described (*17*), and protein dephosphorylation assays were conducted as described above.

Crystallization. Crystals of recombinant $EPPase_{PGM}$ were grown overnight at 4 °C using the hanging drop method by mixing 2 μL of 20 mg/mL $EPPase_{PGM}$ in 20 mM HEPES, 150 mM NaCl, pH = 7.5, 10 mM DTT, and 2 μL of a reservoir solution. The reservoir consisted of 16% (w/v) poly(ethylene glycol)-8000 (PEG8000), 0.2 M $MgCl_2$, 0.2 M NaI, 0.1 M Tris-HCl, pH = 7.5, and 5−40 mM Na_2WO_4. Under the same reservoir conditions and in the absence of tungstate, crystals did not appear. $EPPase_{PGM}$ crystallized in space group $P2_12_12_1$ (a = 62.8 Å, b = 134.2 Å, c = 135.0 Å) with two dimers in the asymmetric unit corresponding to a V_m value (*20*) of 2.49 $Å^3$/Da and an estimated solvent content of 50%.

Data Collection, Structure Determination, and Refinement. Crystals were cryoprotected by increasing the PEG8000 concentration to 30% in 10% ethylene glycol before flash freezing in liquid nitrogen. Diffraction intensities to 1.76 Å were collected at 100 K on beamline X6A at the National Synchrotron Laboratory Source (NSLS), Brookhaven, processed, and scaled with the HKL2000 package (*21*).

The structure of $EPPase_{PGM}$ was solved using the single wavelength anomalous dispersion (SAD) technique. A run consisting of 425° was collected on a single crystal at a wavelength of 1.0 Å to ensure high anomalous signal of the tungsten. The heavy-atom substructure was solved in the program SHELXD (*22*) with data truncated to 2.3 Å resolution. This resolution cut was based on statistics reported by the program SHELXC. Four tungsten atoms were found using this approach. Initial phases calculated with the program SHELXE were improved by density modification in the program DM of the CCP4 package (*23*). The resulting electron density map calculated to 1.76 Å proved to be of excellent quality. This electron density was used to build an initial model of four $EPPase_{PGM}$ monomers with the automatic building procedure in ARP/wARP (*24*). This model was further refined in REFMAC (*25*) to crystallographic residuals R_{cryst}/R_{free} of 19.5/22.9% and excellent stereochemistry. At this stage of the refinement, an ($F_o - F_c$) electron density map clearly showed the presence of positive peaks (≥5σ) that were not water molecules or protein atoms. Five of these peaks were assigned to iodide atoms based on a difference anomalous map, and the rest were modeled as chloride or water molecules. This step reduced the R_{free} residual to 22.0%. One round of translation−libration−screw (TLS) refinement (*26*) improved the R_{cryst}/R_{free} residuals to 18.8/21.0%. The final model lacks density for residues 69−71 in each monomer. Stereochemistry was checked with the program PROCHECK (*27*). Tables 1 and 2 summarize statistics on data collection and model refinement. Coordinates of *B. mori* $EPPase_{PGM}$ have been deposited in the Protein Data Bank under accession number 3C7T.

Table 1: Statistics on Data Collection

unit cell dimensions ($Å^3$)	62.9 × 134.4 × 135.2
space group	$P2_12_12_1$
wavelength (Å)	1.0
resolution (Å)	95.3−1.75
number of observations	4 704 596
number of unique reflections	114 147
completeness, overall (last shell)[a] (%)	99.7 (97.8)[c]
redundancy, overall (last shell)[a]	6.9 (6.3)[c]
$\langle I\rangle/\langle\sigma(I)\rangle$, overall (last shell)[a]	29.6 (2.6)[c]
R_{sym}[b](%)	9.9 (65.4)[c]

[a] Last shell is 1.78−1.75 Å. [b] $R_{sym} = \sum_{i,hkl}|\langle I(hkl)\rangle - I_i(hkl)|/\sum_{i,hkl}I_i(hkl)$. [c] The shown statistics are obtained treating I^+ and I^- as independent reflections in data scaling.

Table 2: Statistics on Model Refinement

resolution (Å)	95.3−1.76
no. of reflections used	108 260
protein atoms	8172
nonprotein atoms	658
B factor ($Å^2$), overall (from Wilson plot)	24.7 (19.2)
R_{free}[a] (%), overall (last resolution shell)	21.0 (24.4)
R_{work}[b] (%), overall (last resolution shell)	18.0 (21.6)
R_{cryst}[c] (%)	18.2
rms deviation in bond length (Å)	0.013
rms deviation in bond angle (deg)	1.39
estimated standard uncertainties[d] (Å)	0.108
Ramachandran plane[e] (%)	93.8/6.0

[a] $R_{free} = \sum_{(hkl)\varepsilon T}||F_{obs}| - |F_{calc}||/\sum_{(hkl)\varepsilon T}|F_{obs}|$, where T is the test set (*38*) obtained by randomly selecting 5% of the data. Last resolution shell is 1.80−1.76 Å. [b] $R_{work} = \sum_{(hkl)\varepsilon W}||F_{obs}| - |F_{calc}||/\sum_{(hkl)\varepsilon W}|F_{obs}|$, where W is the working set. [c] $R_{cryst} = \sum_{(hkl)}||F_{obs}| - |F_{calc}||/\sum_{(hkl)}|F_{obs}|$ calculated over the entire set of unique reflections. [d] Calculated from R_{free} statistics. [e] Most favored/additional allowed regions. Asn98 of chain B and Asp99 of chain C reside in disallowed regions.

Molecular Docking. The Autodock4 suite of programs (*28, 29*) was used for the docking calculations. Ecdysone phosphate (E22P) was built using the program CORINA3D (http://www.molecular-networks.com/) and manually positioned into chain A of $EPPase_{PGM}$. The resultant structure of the complex was relaxed using the module Discover3 of the program package INSIGHT II (http://accelrys.com/) fixing the backbone atoms of the pocket. The consistent valence force field (CVFF) was used for energy minimization, and 2000 steps were applied with default parameters. Here, a distance restraint was specified between the phosphorus atom and atom NE2 of His380. The Autodock Tools (ADT) were used to prepare the minimized protein and ligand, all hydrogen atoms were added, and Gasteiger charges were assigned to the protein. The AM1BCC charges (*30*) were added to E22P using the package Chimera (*31*). The Autogrid with 40 × 40 × 40 grid size with a spacing of 0.375 Å centered on the special position in the binding site was prepared with ADT. Docking was performed using the empirical free energy function and the Lamarckian genetic algorithm applying the following protocol: the energy evaluations were 100 000; the maximum number of iterations was 27 000 for an initial population of 100 randomly placed individuals with a mutation rate of 0.02, a crossover rate of 0.8, and an elitism value of 1. The number of docking runs was set to 10 000, and the results were evaluated by sorting the binding energy predicted by docking conformations. The

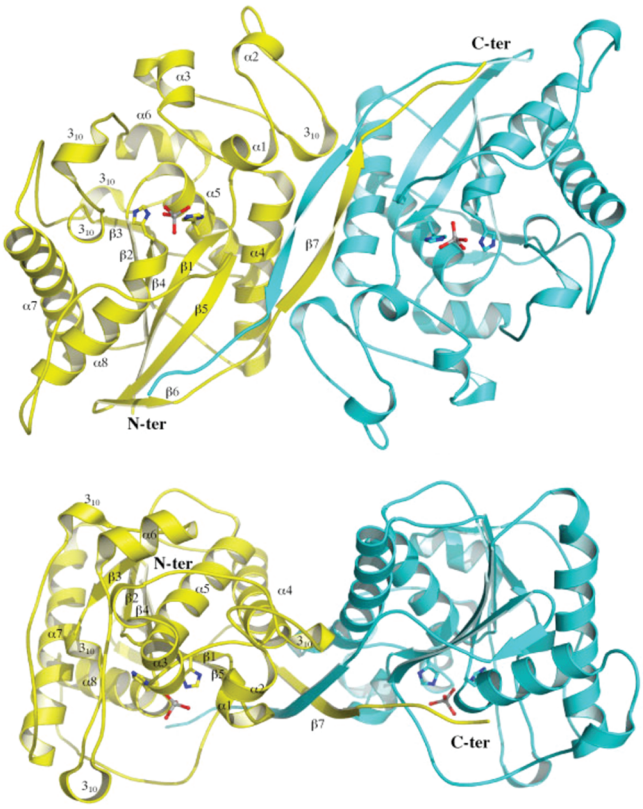

FIGURE 1: Ribbon diagram of the EPPase$_{PGM}$ dimer. In the top view, the dimer's 2-fold axis is perpendicular to the plane of the page, while in the bottom view it is vertical in the plane of the page. Secondary structure elements and termini are indicated for one monomer. The side chains of His80 and His260, as well as the tungstate ions are shown in ball-and-stick representation to locate the active site. Prepared with MOLSCRIPT (*39*) and PYMOL (http://pymol.sourceforge.net/).

results were clustered with a tolerance of 2.0 Å. The standard error on these calculations is ~2.5 kcal/mol.

RESULTS

Overall Structure of the EPPase$_{PGM}$. To gain insight into the steroid phosphate phosphatase activity of *B. mori* EPPase$_{PGM}$, we crystallized this domain and solved its three-dimensional structure by X-ray crystallography. The crystals contain four molecules in the asymmetric unit organized into two dimers. The dimeric structure of EPPase$_{PGM}$ in the crystal is consistent with the size exclusion data (not shown).

The rms deviations calculated after superposing the Cαs of all four EPPase$_{PGM}$ monomers on each other range between 0.29 and 0.50 Å indicating that all monomers are identical. The EPPase$_{PGM}$ monomer has an α/β structure similar to that adopted by members of the 2H-phosphatase superfamily (*13, 14*). A central six-stranded β-sheet forms the core of the monomer and is surrounded by eight α-helices and four 3_{10}-helices. The C-terminal tail of each monomer (residues 310−330) extends outside of the core and makes strong interactions with the second monomer of the dimer (Figure 1). The ^{79}RHGE^{82} signature motif is located in a cavity formed by the carboxyl end of the central β-sheet and by surrounding loops. This cavity is solvent-exposed and contains the conserved Arg160 and His260 in addition to the signature motif. These residues are conserved in all 2H-phosphatases and have been shown to be the key catalytic residues in these enzymes (*13, 14*). Thus, the surface cavity that lies at the carboxyl end of the β-sheet likely constitutes the active site of EPPase. The conservation of key catalytic residues suggests a conservation of the catalytic mechanism between EPPase and the 2H-phosphatases (see below and Scheme 2).

Structural Comparison to Other 2H-Phosphatases. Having established that EPPase$_{PGM}$ is structurally related to members of the 2H-phosphatase superfamily, we compared its structure to that of other 2H-phosphatases. The bacterial phosphatase SixA is the smallest member in the superfamily. Its structure in complex with tungstate is available (*32*), permitting a comparison to the tungstate-bound structure of EPPase$_{PGM}$. Superposition of the two proteins (*33*) reveals an rms deviation of 1.7 Å calculated over 129 superposable Cα atoms out of SixA's 161. This superposition leads to a structure-based sequence alignment between the two proteins (Supporting Information). The core is well conserved between the two enzymes. The differences lie in three secondary structure connecting loops, namely, the ones connecting β1 to α3 (residues 86−124), β3 to α7 (residues 189−236), and α8 to β5 (residues 272−292) (Figure 2A and Supporting Information). The first two loops are absent in SixA. Interestingly, the structure of several 2H-phosphatases contains two inserts after β1 and β3 as opposed to SixA's minimal topology. In addition to the three loops, the C-termini of EPPase$_{PGM}$ (residues 311−330) and SixA (residues 149−161) adopt different conformations and do not superpose on each other (green in Figure 2A).

EPPase is highly homologous to the 2H-phosphatase Sts-1. In turn, this primary amino acid sequence homology leads to close structural homology between the PGM domains of the two proteins (Figure 2 and Supporting Information). The rms deviation calculated after superposing EPPase$_{PGM}$ and Sts-1$_{PGM}$ (*33*) is 1.20 Å for 224 equivalent Cα atoms out of 260. Those inserts that differ topologically between SixA and EPPase$_{PGM}$ superpose well between EPPase$_{PGM}$ and Sts-1$_{PGM}$ (blue and crimson in Figure 2A), although there are subtle structural differences that might be important for substrate specificity (Figure 2B and later).

Unlike the C-terminus of SixA, both C-termini of EPPase$_{PGM}$ and Sts-1$_{PGM}$ (green in Figure 2A) lie at the dimer interface. In this regard, inspection of the Protein Data Bank with the program PISA (*34*) shows that EPPase$_{PGM}$ dimerizes in a similar fashion to Sts-1$_{PGM}$ but differently from the manner in which other known 2H-phosphatases dimerize, despite similarity in the overall fold (*17*). Six regions of EPPase$_{PGM}$ are involved in the dimer interface (Figure 3A): residues 86−88 of helix-α1, 103−110 of insert 1, 130−145 of helix-α4, 264−268 of helix-α8, 288−300 at the end of insert 3, and the C-terminal residues 308−330 (loop β6/β7 and strand β7), which makes the majority of the dimer interface. In addition, isolated residues such as Glu82, His272, and Gln282 are also part of the dimer interface. The dimer interface protects 2370 Å^2 of accessible surface area and is hydrophobic in character since 64% of the atoms at the interface are apolar while the remainding ones are polar. More importantly, the EPPase$_{PGM}$ dimer interface is unique in its location and extent when compared with other 2H-phosphatases (*17*). This suggests that EPPase and Sts-1 are more related to one other than to other members of the 2H-phosphatase superfamily.

Scheme 2: Schematic Representation of the Proposed Reaction Mechanism of EPPase[a]

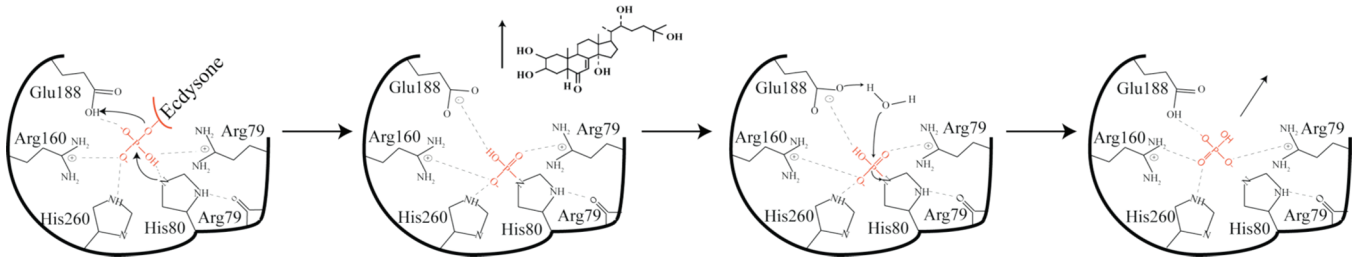

[a] Only catalytic residues are shown. See text for more details.

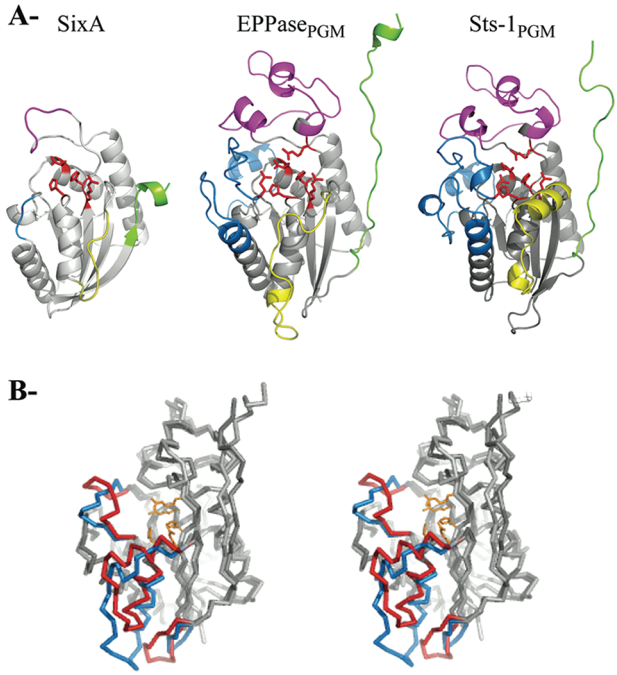

FIGURE 2: Comparison of *B. mori* EPP$_{PGM}$, SixA, and Sts-1$_{PGM}$. (A) SixA (PDB ID 1UJC), EPPase$_{PGM}$, and mSts-1$_{PGM}$ (PDB ID 2H0Q) monomers are shown in ribbon representation in similar orientations. Conserved catalytic residues are shown in red ball-and-stick: the histidines (H8/H108 in SixA, H80/H260 EPPase$_{PGM}$, and H380/H565 in mSts-1$_{PGM}$), the arginines (R7/R55 in SixA, R79/R83/R160 in EPPase$_{PGM}$, and R379/R383/R462 in mSts-1$_{PGM}$), and the glutamates (E188 in EPPase$_{PGM}$, and E490 in mSts-1$_{PGM}$). The secondary structure elements that are conserved among the three proteins are in gray. The regions that deviate between SixA and EPPase$_{PGM}$ are in crimson (insert 1), blue (insert 2), and yellow (insert 3). The C termini are in green. (B) Stereoview of overlaid Cα atoms of EPPase$_{PGM}$ (light gray) and mSts-1PGM (dark gray). The three regions that deviate between EPPase$_{PGM}$ (residues 192−197, 272−292) and Sts-1PGM (residues 494−500, 575−593, 607−610) and shaded in gray in Supporting Information are colored in red and blue, respectively. Conserved active site residues are shown in gold to highlight the phosphate-binding site.

The EPPase$_{PGM}$ Phosphate-Binding Site. The structural similarity between EPPase$_{PGM}$, Sts-1$_{PGM}$, and other 2H-phosphatases is particularly strong within the catalytic residues in the active site. As noted above, the EPPase residues His80, His260, Arg79, and Arg160 that are strictly conserved with other members of the 2H-phosphatase superfamily (Supporting Information) cluster together at this site. As in other 2H-phosphatases, His80 is stacked against Arg79 and Arg160 (Figure 3B). In addition, other conserved interactions ensure that the catalytic cavity adopts the same structure as in many other 2H-phosphatases. For example, the backbone amino group of Gly81 (Gly9 in SixA) makes a hydrogen bond with the side chain hydroxyl group of the conserved Thr164 (Thr59 in SixA) while its carbonyl group interacts with His80. In the conserved ^{127}PLTRLG^{132} motif (^{23}PLTTNG^{27} in SixA), the Leu128 side chain contacts His80, Gly81, and Arg160 while the hydroxyl side chain of Thr129 makes hydrogen bonds with the side chain of Glu82 of the ^{79}RHGE^{82} motif as well as with the backbone amino group of Gly132. The hydroxyl side chain group of the conserved Ser156 (Ser51 in SixA) is within a hydrogen bond distance from His260, while Pro157 (Pro52 in SixA) introduces a sharp turn at the end of strand β2 leading the polypeptide into helix α5.

The four conserved histidine and arginine residues are complemented in the active site of EPPase$_{PGM}$ by another basic residue, Arg83. The presence of numerous basic residues gives the active site of EPPase$_{PGM}$ a strongly basic positive potential (Figure 3C). Other factors are also likely to contribute to the positive potential of the EPPase$_{PGM}$ active site. For example, helix α8 is oriented such that its N-terminus points toward the end of the β-sheet where His80 is located (Figure 1) and the dipole moment of this α-helix likely contributes to the positive potential in the active site. Together, the active site basic residues and the α8 dipole moment synergize to attract and stabilize a negatively charged group such as a phosphate.

Four EPPase$_{PGM}$ residues found within the catalytic pocket, Glu82, Arg83, Glu188, and Tyr295 are conserved in Sts-1 (Glu382, Arg383, Glu490, and Tyr596) but not in SixA. These residues are close to the tungstate moiety (see below) or border the catalytic pocket and therefore are believed to play an important role in catalysis. For example, the side chain of Arg83 (Ala11 in SixA) makes hydrogen bonds with the tungstate and is stabilized by Asp85 (Asp385 in Sts-1). In SixA however, the guanidium group of Arg21 is well positioned to play the role of Arg83 in EPPase$_{PGM}$. Water molecules mediate the interaction between the tungstate and the side chain of Glu188 (Pro81 in SixA), the only acidic residue in the active site. The side chain of Glu82 of the ^{79}RHGE^{82} motif points away from the catalytic pocket and makes hydrogen bonds with the side chains of Asn107 and Thr129 as well as with Ser310 from the other monomer of the dimer. The side chain of Tyr295 (Thr130 in SixA) is positioned close to His80 and its function is unclear. The conservation of these active site residues between EPPase and Sts-1 but not in SixA suggests a common set of substrates between the former two enzymes but not with SixA.

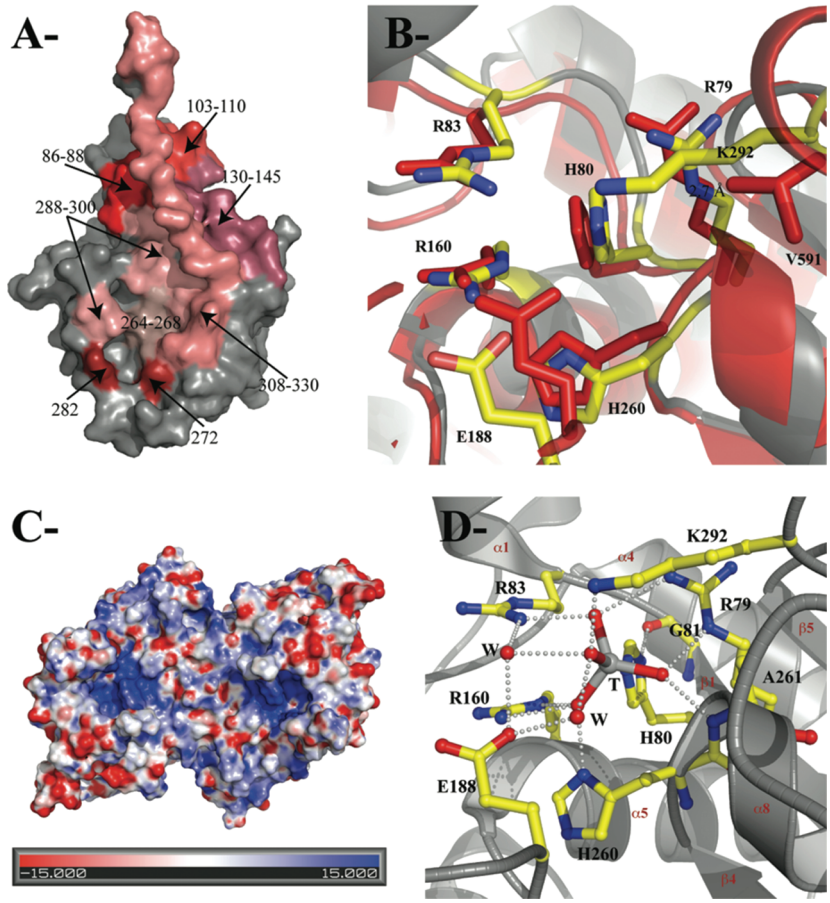

FIGURE 3: Dimerization and phosphate-binding site. (A) $EPPase_{PGM}$ is shown in surface representation in gray. Polypeptides and single residues (272 and 282) at the dimer interface are colored in shades of red and indicated. (B) Superposition of the $EPPase_{PGM}$ active site residues (yellow) with their equivalents in Sts-1_{PGM} (red). (C) $EPPase_{PGM}$ oriented as in Figure 1 top view and displayed in its Connolly surface is colored according to its electrostatic potential contoured from −15 (intense red) to 15 k_BT/e (intense blue). (D) Interactions made by the tungstate (T) ion and $EPPase_{PGM}$. Active site residues within hydrogen-bonding distances of the tungstate ion are shown in ball-and-stick. Dashed lines represent hydrogen-bond interactions and red spheres water molecules (W).

The conservation in the primary and tertiary structures of the active site between EPPase and the 2H-phosphatases suggests that the mechanism of substrate dephosphorylation is also conserved between these proteins. According to this mechanism, His80 conducts an in-line nucleophilic attack on the phosphorylated substrate and becomes transiently phosphorylated during catalysis. The release of the dephosphorylated substrate into the solvent is followed by the hydrolysis of phosphorylated-His80 by an activated water molecule to produce free phosphate and the enzyme is available for a new cycle of activity (Scheme 2) (*13, 14*). The strong hydrogen bond between ND1 of His80 and the main chain carbonyl of Gly81 ensures that ND1 is protonated, thereby leaving NE2 deprotonated and capable of nucleophilic attack on a phosphate group (Figure 3D). The conserved Arg79/Arg83/Arg160/His260 are predicted to stabilize the structures of the transition states during catalysis, while Glu188 and His260 are involved in the subsequent dephosphorylation of the phosphoenzyme. In support of this proposed scheme, we found a tungstate ion trapped in all four chains in the middle of the active site with the tungsten atom at 2.40 to 2.50 Å from NE2 of His80. It is stabilized by a network of hydrogen bonds with the side chains of the basic residues Arg79, His80, Arg83, Arg160, Glu188, His260, and Lys292 and the main chain amino group of Ala261 (Figure 3D). These interactions are tighter than those made between the tungstate ion and the active site of SixA (*32*). Except for Lys292, which has no equivalent in Sts-1 or other 2H-phosphatases, the residues that stabilize the tungstate ion adopt an identical conformation in apo-Sts-1_{PGM} (Figure 3B) implying that the active site is rigid and does not change its conformation upon the binding of substrates. This conclusion is supported by the observation that the catalytic residues are also involved in a network of hydrogen bonds with neighboring EPPase residues.

Although the overall PGM domains of EPPase and Sts-1 superpose well, there are significant sequence differences in residues bordering the proposed active site of each enzyme. Specifically, residues 191−199 at the N-terminus of insert 2 and residues 272−292 of insert 3 (Supporting Information) that connect α8 to β6 form two loops in EPPase at opposite sides of the phosphate binding site that structurally deviate from their counterparts in Sts-1 (residues 493−502 and 577−593). As shown in Figure 4, the conformation of these two loops creates an open, solvent-exposed cavity in $EPPase_{PGM}$. In contrast, the same cavity on the surface of Sts-1_{PGM} is filled with the bulky aliphatic side chains of Trp491, Trp494, Phe587, Val588, and Val591 restricting the access to this pocket in Sts-1_{PGM}. The equivalent residues in $EPPase_{PGM}$ are either pointing to the solvent, as is the case of Trp192 and Leu290 or are less bulky as in the case of Phe189.

The Putative Ecdysone Phosphate-Binding Site. The EPPase structure does not show a cavity similar to the

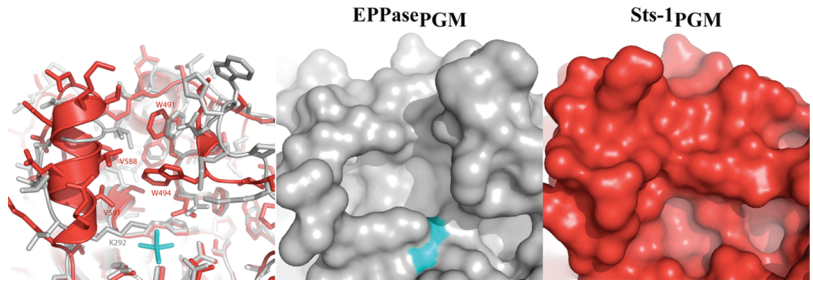

FIGURE 4: Comparison of the surroundings of the phosphate-binding site in EPPase$_{PGM}$ and Sts-1$_{PGM}$. EPPase$_{PGM}$ (gray) and Sts-1$_{PGM}$ (red) were superposed (*33*), overlaid, and shown in stick or surface representations. The tungstate ion is shown in cyan. Hydrophobic residues of Sts-1$_{PGM}$ that block the access to a cavity that is otherwise solvent-exposed in EPPase$_{PGM}$ are labeled in red.

ecdysone-binding site found in the EcR (*35*) suggesting that it represents the prototype of a new ecdysone-binding site. To investigate where in the EPPase structure the ecdysone phosphate binds, we docked the steroid phosphate molecule using the program Autodock (*28*) into the EPPase structure from which we removed the tungstate. As modeled (Figure 5), the steroid phosphate sits in the solvent-exposed pocket located at the C-terminal end of the β-sheet and replaces eight structural water molecules found in the tungstate bound structure. To accommodate the ecdysone phosphate the side chains of Lys196 and Lys292 had to adopt a new rotamer conformation while the rest of the pocket retained its structure. In this configuration, the calculated free energy of binding of the ecdysone phosphate is −6.41 kcal/mol. The ecdysone phosphate makes several hydrogen bond and van der Waals interactions with the protein. For example, the side chain of the ecdysone is stabilized by the side chains of Glu188, Ile262, and Lys292 and by hydrogen bonds between its hydroxyl group and the main chain amino groups of Ala261 and Ile262. In addition, the phosphate moiety at position 22 makes hydrogen bonds with the side chains of Arg79, His80, and His260. This moiety is positioned close to the nucleophilic His80 in the same site that is occupied by the tungstate such that the phosphorus atom is 2.94 Å from the deprotonated NE2. The ring structure of the steroid makes several hydrogen bonds through its hydroxyl groups with the main chain carbonyl groups of Lys124 and Gly197 and the side chains of Arg160, Glu188, and Lys196. In addition, the ring structure is partly protected from the solvent by the long side chain of Lys196. This pocket is conserved between EPPase and Sts-1 with one difference. In Sts-1, the bulky side chain of Trp494 clashes with the E22P side chain suggesting that Sts-1 will hydrolyze E22P less efficiently.

Phosphatase Activity of the Recombinant B. mori EPPase$_{PGM}$. Given that the full-length EPPase showed a phosphatase activity (*9*), we investigated whether recombinant EPPase$_{PGM}$ retained this activity. EPPase$_{PGM}$ was tested for its ability to hydrolyze the nonspecific phosphatase substrate *p*NPP. *p*NPP has been shown to be a substrate of EPPase and a competitive inhibitor of E22P (*9*). A time course of EPPase$_{PGM}$-catalyzed *p*NPP hydrolysis at different substrate concentrations (50 μM to 10 mM) demonstrated that recombinant EPPase$_{PGM}$ is capable of dephosphorylating *p*NPP with kinetics that resemble a Michaelis−Menten enzyme-catalyzed reaction. Initial reaction velocities at each *p*NPP concentration were measured and plotted (Figure 6A). Fitting of the data points to eq 1 resulted in a K_m value of 1.9 ± 0.2 mM for the *p*NPP and a turnover number k_{cat} of 11.7 ± 0.6 s^{-1}. These values are 7 and 11 times lower than

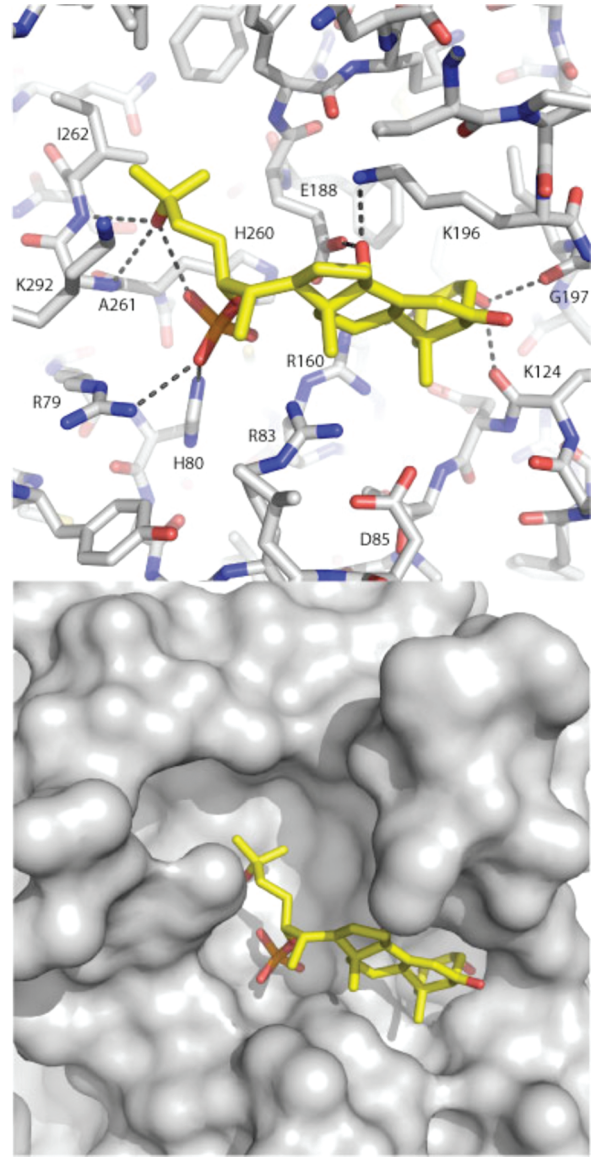

FIGURE 5: Putative E22P binding site. Docking of E22P to EPPase$_{PGM}$ orientated as in Figure 4, was done with Autodock (*28*). Hydrogen bond interactions between E22P and its proposed binding pocket shown in stick and surface representation are shown as dotted lines.

the previously reported values for the native or recombinant full-length protein but result in a k_{cat}/K_m ratio that is very comparable (6000 versus 10 300 M^{-1} s^{-1}, Table 3). In comparison, the k_{cat} and k_{cat}/K_m values of EPPase$_{PGM}$ are 6-fold and 20-fold slower than that of the homologous Sts-1$_{PGM}$ (Table 3). Mutation of His80 to serine completely

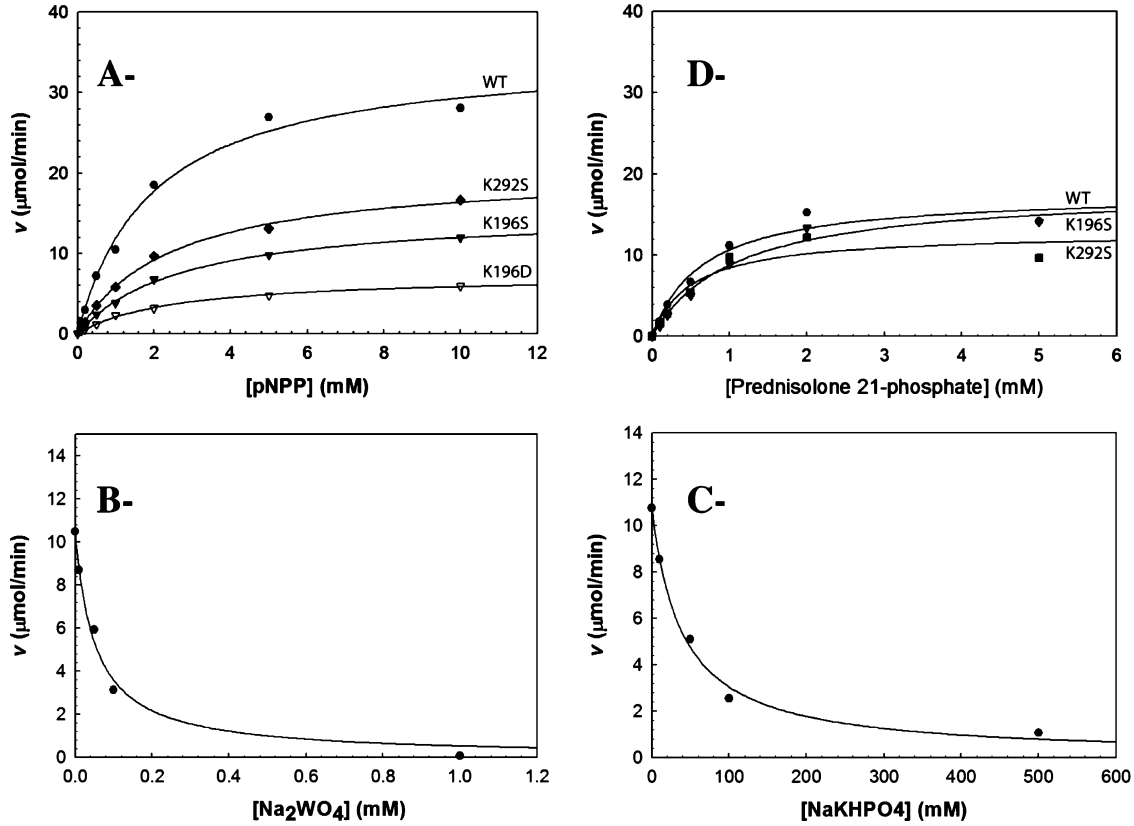

FIGURE 6: Phosphatase activity of recombinant *B. mori* EPPase$_{PGM}$. (A) Assays were carried out with 50 nM EPPase$_{PGM}$ wild-type, K196S, K196D, or K292S mutants and *p*NPP at various concentrations. K_m and k_{cat} were obtained after fitting the data points to eq 1. Inhibition of EPPase$_{PGM}$ activity by (B) tungstate or (C) phosphate. Initial velocities of *p*NPP hydrolysis by EPPase$_{PGM}$ were measured and plotted at the indicated tungstate or phosphate concentrations (●). The data points were fitted to eq 2. All assays were conducted at pH 7.5 and 37 °C. (D) Phosphatase activity assay was carried out as in panel A with prednisolone 21-phosphate as substrate.

Table 3: Comparison of the Phosphatase Activity of Sts-1$_{PGM}$ and EPPase$_{PGM}$

substrate/enzyme	k_{cat} (s^{-1})	K_m (mM)	k_{cat}/K_m (M^{-1} s^{-1})	activity (%)[a]
*p*NPP				
Sts-1$_{PGM}$	70.1	0.5 ± 0.07	140 000	8 400
EPPase$_{PGM}$	11.7	1.9 ± 0.2	6 000	100
EPPase$_{PGM}$ H80S	*b*	*b*		
EPPase$_{PGM}$ K196S	5.0	2.7 ± 0.16	1 873	31
EPPase$_{PGM}$ K196D	2.4	2.5 ± 0.2	984	16
EPPase$_{PGM}$ K292S	6.3	2.4 ± 0.2	2 625	50
pTyr				
EPPase$_{PGM}$	7.5	3.6	2 083	34.7
prednisolone 21P				
Sts-1$_{PGM}$	0.15	0.45 ± 0.09	334	6
EPPase$_{PGM}$	5.9	0.65 ± 0.17	9 014	150
EPPase$_{PGM}$ H80S	*b*	*b*		
EPPase$_{PGM}$ K196S	6.1	1.06 ± 0.24	5 666	94
EPPase$_{PGM}$ K292S	4.2	0.51 ± 0.23	8 327	139
dexamethasone 21P				
EPPase$_{PGM}$	3.44	2.0 ± 0.14	1 721	29
β-methasone 21P				
EPPase$_{PGM}$	10.2	0.73 ± 0.32	14 029	234
EPPase[c](*p*NPP)	135	13.1	10 300	
EPPase[c](E22P)	0.94	0.0059	161 000	

[a] EPPase$_{PGM}$ activity against *p*NPP is used as a reference (100%). [b] Not detectable. [c] Values taken from ref *9*.

Table 4: IC_{50} and K_I Values (μM) of Various EPPase$_{PGM}$ Inhibitors Measured with 1 mM *p*NPP

	EPPase$_{PGM}$	
inhibitor	IC_{50}	K_I
tungstate	52	34
vanadate	2 906	1 900
phosphate	47 066	25 770

abolishes the phosphatase activity of EPPase$_{PGM}$ consistent with the role of His80 as a key catalytic residue during hydrolysis. Tungstate, vanadate, and phosphate, which are common phosphatase inhibitors slowed down the activity of EPPase$_{PGM}$ (Figure 6B,C). Fitting the initial rates of *p*NPP hydrolysis plotted versus the inhibitor concentration to eq 2 reveals that the IC_{50} of tungstate is 52 ± 0.8 μM while the IC_{50}'s of vanadate and phosphate are 2.9 ± 0.43 and 47 ± 11 mM, respectively (Table 4). In accordance with previous data (*9*), L-tartrate, a common inhibitor of PGM proteins did not inhibit *p*NPP hydrolysis by EPPase$_{PGM}$ even when concentrations as high as 100 mM were used in the assay.

Given that EPPase was cloned based on its ability to dephosphorylate E22P (*9*), we assessed the ability of recombinant EPPase$_{PGM}$ to dephosphorylate various steroid phosphates. Prednisolone 21-phosphate, a steroid phosphate that resembles E22P although with a shorter side chain, was shown to be substrate for EPPase (*15*). EPPase$_{PGM}$ (50 nM) hydrolyzes prednisolone 21-phosphate, dexamethasone 21-phosphate, and β-methasone 21-phosphate. Fitting of the data points to eq 1 resulted in K_m values of 0.65 ± 0.17, 2.0 ± 0.14, and 0.73 ± 0.32 mM and turnover numbers k_{cat} of 5.9, 3.44, and 10.2 s^{-1}, respectively (Table 3). By comparison, a higher Sts-1$_{PGM}$ concentration (500 nM) was needed to detect dephosphorylation. In addition, the k_{cat}/K_m ratio for prednisolone 21-phosphate dephosphorylation is 27-times higher for EPPase$_{PGM}$ than for Sts-1$_{PGM}$, a result that is mainly due to a higher turnover number (5.9 vs 0.15 s^{-1}). Taken together,

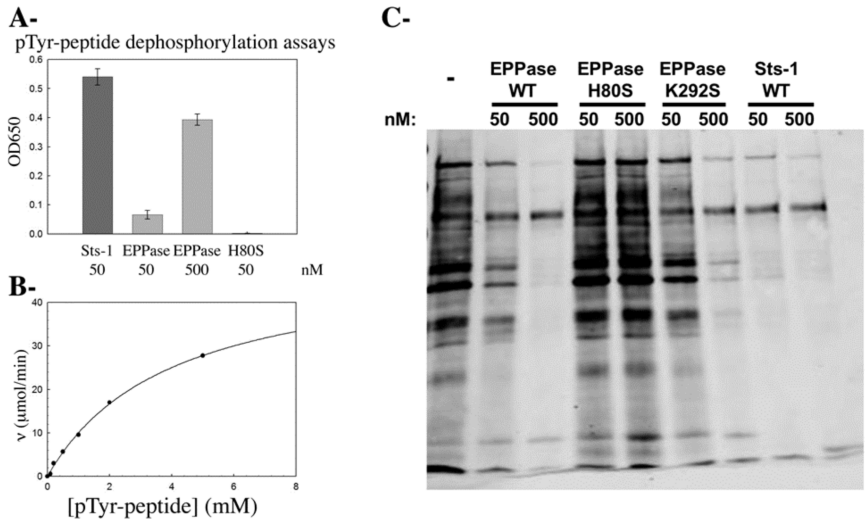

FIGURE 7: PTP activity of $EPPase_{PGM}$. (A) Dephosphorylation of a pTyr-containing peptide by wild-type, H80S mutant $EPPase_{PGM}$, and Sts-1_{PGM} (50 and 500 nM). The concentration of the released phosphate was measured using the malachite green assay read at 650 nm. (B) Plot of the initial rate of hydrolysis vs the pTyr-peptide concentration. (C) Proteins from TCR-stimulated Jurkat cells were isolated by immunoprecipitation, eluted from the pTyr antibodies, and evaluated as $EPPase_{PGM}$ substrates at the indicated concentration. Reaction products were evaluated by anti-phosphotyrosine Western analysis. All assays were conducted at pH 7.5 and 37 °C. Each assay was repeated at least three times. Figures are representative of one experiment.

our biochemical data suggest that despite the structural and sequence homology Sts-1_{PGM} and $EPPase_{PGM}$ exhibit different substrate specificity.

Probing the role of Lys292 and Lys196 in Catalysis. Close inspection of the $EPPase_{PGM}$ active site reveals the presence of a lysine residue (Lys292) that is not conserved in any other known 2H-phosphatase. The side chain amino group of Lys292 is within 2.7 Å from a tungstate oxygen implying a strong hydrogen bond with the phosphate analogue (Figure 3D). This observation in conjunction with the docking results that showed the side chains of Lys292 and Lys196 close to E22P raises the possibility that these two lysines play a unique role in the EPPase phosphatase reaction. To test this hypothesis, we cloned and purified the (K196S, K196D) and K292S mutants of $EPPase_{PGM}$ and evaluated their phosphatase activity. As shown in Figure 6A,D and Table 3, the two lysine mutants hydrolyze *p*NPP with a 2−5 times lower k_{cat} constant than wild-type but prednisolone-21P with kinetic constants similar to those of the wild-type $EPPase_{PGM}$. We also tested the ability of tungstate to inhibit the activity of the K292S mutant and found that under the same conditions used for the wild-type protein the IC_{50} of tungstate is 70 μM for the K292S mutant similar to the 52 μM found for the wild-type $EPPase_{PGM}$. Taken together, these data show that despite the tight interaction with the tungstate, Lys292 and Lys196 contribute modestly to the phosphatase reaction. They also imply that the strictly conserved arginine and histidine residues lining the active site suffice for the catalytic activity. Likely, the positively charged Lys292 side chain is nonspecifically attracted to the tungstate anion hole.

Substrate Specificity of $EPPase_{PGM}$. Many 2H-phosphatases exhibit stringent substrate specificity while others are promiscuous. To evaluate $EPPase_{PGM}$ substrate specificity, we tested different phosphorylated compounds as substrates. We incubated $EPPase_{PGM}$ with a variety of phosphorylated small molecules that can be dephosphorylated by the promiscous human prostatic acid phosphatase, hPAcP (*36, 37*). $EPPase_{PGM}$ (50 nM) was incubated under standard reaction conditions with 1 mM fructose-6-phosphate, β-ribose-5-phosphate, inosine-5-monophosphate, 1-naphtyl phosphate, β-glucose-6-phosphate, and β-phosphoglycerol at pH 7.5. Compared with *p*NPP, which was used as a positive control, $EPPase_{PGM}$ failed to dephosphorylate any of the phosphorylated small molecules (data not shown), thus exhibiting the characteristics of an enzyme with defined substrate specificity.

The close structural similarities between $EPPase_{PGM}$ and Sts-1_{PGM} and the fact that Sts-1_{PGM} acts as a PTP led us to examine whether $EPPase_{PGM}$ had a PTP activity. First, we tested the following pTyr-containing peptide (NH_2-SVYESP-pY-SDPEE-COOH). As illustrated in Figure 7A, recombinant $EPPase_{PGM}$ (50 nM) was able to dephosphorylate the phosphopeptide (1 mM). By comparison, the level of dephosphorylation is approximately ten times less than that of Sts-1_{PGM}. The Sts-1_{PGM} level of dephosphorylation can be reached when a higher $EPPase_{PGM}$ (500 nm) concentration is used. To characterize the kinetics of $EPPase_{PGM}$ dephosphorylation of the pTyr-peptide, we followed the time course of the dephosphorylation reaction at different peptide concentrations (0.1−5 mM). Initial reaction velocities at each peptide concentration were measured and plotted as a function of the peptide concentration (Figure 7B). Fitting of the data points to eq 1 resulted in a K_m value of 3.6 ± 0.7 mM and a turnover number $k_{cat} = 7.5 \pm 1.4\ s^{-1}$ yielding a specificity constant (k_{cat}/K_m) = 2083 $M^{-1}\ s^{-1}$ for the pTyr-peptide. These kinetic constants are comparable to the constants measured for *p*NPP and the steroid phosphates (Table 3) but differ from the reported constants for E22P (*9*). For example, the specificity constant (k_{cat}/K_m) for E22P was found to be 161 000 $M^{-1}\ s^{-1}$, which is 80-times higher than that measured for the pTyr-peptide. This result suggests that EPPase has a higher specificity for the conjugated steroid. This higher specificity is primarily due to the 610-times lower K_m for E22P (5.9 μM) than for the pTyr-peptide (3.6 mM) even though the k_{cat} for the E22P is 8 times lower than that of the pTyr-peptide. However, one should keep in mind that the sequence of the pTyr-peptide used in this study is that of a random peptide and not of an $EPPase_{PGM}$

optimized one. We thus expect higher values for the specificity constant for optimized peptides. Such discrepancy was noted when different peptides were tested as substrates for Sts-1_{PGM} (N.C., unpublished data).

Next, we tested the phosphatase activity of $EPPase_{PGM}$ against pTyr-containing proteins. Tyrosine-phosphorylated proteins were obtained from TCR-stimulated T cells by immunoprecipitation and evaluated as substrates of recombinant $EPPase_{PGM}$. As shown in Figure 7C, both wild-type and K292S mutant of $EPPase_{PGM}$ dephosphorylated pTyr-containing proteins in a dose-dependent manner, while the H80S mutant showed no activity even when used at high concentrations. These observations are consistent with the data presented in Table 3, namely, that His80 is a key catalytic residue while Lys292 is not critical for catalysis. $EPPase_{PGM}$ appeared less efficient than Sts-1_{PGM}, as judged by the need to utilize 10-fold more $EPPase_{PGM}$ enzyme to achieve similar levels of dephosphorylation by Sts-1_{PGM}. The need for higher $EPPase_{PGM}$ concentrations to reach Sts-1_{PGM} levels of dephosphorylation for the substrates *p*NPP, pTyr-peptide, and pTyr-proteins shows that EPPase is a less efficient pTyr-phosphatase than Sts-1. Thus, in addition to being a steroid phosphate phosphatase, EPPase possesses an intrinsic PTP activity *in vitro*.

CONCLUSION

In the present work, we determined the crystal structure of the first steroid phosphate phosphatase and characterized its activity using *in vitro* assays. Consistent with the presence of a ^{79}RHGE^{82} signature motif, our structural and biochemical data demonstrate that EPPase belongs to the 2H-phosphatase family of enzymes. This result is supported by the finding that the structures of the EPPase and the bacterial 2H-phosphatase SixA are related with conservation of both key catalytic residues as well as key interactions that hold the active site together. These conserved residues stabilize the phosphate of the substrate through tight hydrogen bonds as seen with the tungstate moiety, and mutating one of them, namely, His80, dramatically reduces the phosphatase activity of EPPase. Among the 2H-phosphatases, EPPase is structurally and functionally more related to the Sts proteins than to any other family member. This homology has several implications and raises a few questions on the actual function(s) of EPPase.

First, our biochemical and structural data raise the possibility that EPPase, which was initially cloned based on its ability to dephosphorylate ecdysone phosphate *in vitro* might also function as a PTP. The finding that EPPase hydrolyzes tyrosine-phosphorylated proteins and pTyr-like substrates including pTyr-peptides and *p*NPP while small non-pTyr-like molecules are not substrates for EPPase supports the latter idea. Our data thus suggest that EPPase's activity could serve at least two purposes: to activate ecdysone regulated signaling pathways and to down-regulate cellular signaling pathways downstream of a protein tyrosine kinase. In the absence of the structure of a complex between EPPase and a substrate, the reason for the selective specificity of $EPPase_{PGM}$ toward phosphorylated substrates is not well understood. Interestingly, EPPase is inhibited by known PTP inhibitors such as tungstate, vanadate, and phosphate. From a structural point of view, the homology to Sts-1, which was shown to be a PTP, also speaks to a potential PTP role for EPPase. The solvent accessibility of the $EPPase_{PGM}$ active site, which was also noted for Sts-1 and SixA both of which have phosphorylated proteins as substrates, is in accordance with a large substrate. These structural arguments however, do not prove that EPPase is a PTP since Sts-2, an Sts-1 isoform, which structurally resembles Sts-1 more than EPPase does, has even a weaker PTP activity (Y.C., N.C., N.N to be published, ref *17*). Whether the PTP activity of EPPase is relevant *in vivo* remains to be examined.

Second, despite the strong structural and sequence homology between the PGM domains of Sts-1 and EPPase especially in the active site, Sts-1 is a better PTP whereas EPPase is a better steroid phosphate phosphatase. Very likely, nonconserved residues surrounding the active site are responsible for this difference in activity.

Third, a noteworthy aspect of the structural homology between $EPPase_{PGM}$ and Sts-1_{PGM} is the way they dimerize. As illustrated in Figure 1, the C-terminal tails of each monomer intercalate with one another. The specific interactions formed by these contacts that lead to EPPase dimerization appear to be unique among the 2H-phosphatases. The functional significance of this mode of dimerization is unclear, especially in the context of a small substrate like a steroid phosphate that can be fully recognized by a monomeric EPPase. We suggest that in ways yet unknown, the dimerization of EPPase is directly related to its physiological function and the nature of its substrate(s). This is an area of ongoing research in our laboratories. Regardless, it is likely that EPPase and Sts proteins evolved from a common ancestral 2H-phosphatase and that based on their interesting mode of dimerization they likely constitute a distinct subgroup within the 2H-phosphatase family.

ACKNOWLEDGMENT

We thank Ben Sondgeroth for expert technical assistance, Todd Miller and Mark Bowen for helpful discussions and comments on the manuscript, and Vivian Stojanoff for help with data collection at X6A.

SUPPORTING INFORMATION AVAILABLE

Structure-based sequence alignment of the three 2H-phosphatases EPPase, Sts-1, and bacterial SixA. This material is available free of charge via the Internet at http://pubs.acs.org.

REFERENCES

1. Gelman, D. B., Pszczolkowski, M. A., Blackburn, M. B., and Ramaswamy, S. B. (2007) Ecdysteroids and juvenile hormones of whiteflies, important insect vectors for plant viruses. *J. Insect Physiol. 53*, 274–284.
2. Mirth, C. K., and Riddiford, L. M. (2007) Size assessment and growth control: How adult size is determined in insects. *Bioessays 29*, 344–355.
3. Yin, V. P., and Thummel, C. S. (2005) Mechanisms of steroid-triggered programmed cell death in *Drosophila*. *Semin. Cell Dev. Biol. 16*, 237–243.
4. Dubrovsky, E. B. (2005) Hormonal cross talk in insect development. *Trends Endocrinol. Metab. 16*, 6–11.
5. Sonobe, H., and Yamada, R. (2004) Ecdysteroids during early embryonic development in silkworm *Bombyx mori*: Metabolism and functions. *Zool. Sci. 21*, 503–516.
6. Nijhout, H. F. (2003) The control of body size in insects. *Dev. Biol. 261*, 1–9.

7. Makka, T., Seino, A., Tomita, S., Fujiwara, H., and Sonobe, H. (2002) A possible role of 20-hydroxyecdysone in embryonic development of the silkworm *Bombyx mori*. *Arch. Insect Biochem. Physiol. 51*, 111–120.
8. Thummel, C. S., and Chory, J. (2002) Steroid signaling in plants and insects--common themes, different pathways. *Genes Dev. 16*, 3113–3129.
9. Yamada, R., and Sonobe, H. (2003) Purification, kinetic characterization, and molecular cloning of a novel enzyme ecdysteroid-phosphate phosphatase. *J. Biol. Chem. 278*, 26365–26373.
10. Caldwell, P. E., Walkiewicz, M., and Stern, M. (2005) Ras activity in the *Drosophila* prothoracic gland regulates body size and developmental rate via ecdysone release. *Curr. Biol. 15*, 1785–1795.
11. Colombani, J., Bianchini, L., Layalle, S., Pondeville, E., Dauphin-Villemant, C., Antoniewski, C., Carre, C., Noselli, S., and Leopold, P. (2005) Antagonistic actions of ecdysone and insulins determine final size in *Drosophila*. *Science 310*, 667–670.
12. Mirth, C., Truman, J. W., and Riddiford, L. M. (2005) The role of the prothoracic gland in determining critical weight for metamorphosis in *Drosophila melanogaster*. *Curr. Biol. 15*, 1796–1807.
13. Rigden, D. J. (2008) The histidine phosphatase superfamily: Structure and function. *Biochem. J. 409*, 333–348.
14. Jedrzejas, M. J. (2000) Structure, function, and evolution of phosphoglycerate mutases: Comparison with fructose-2,6-bisphosphatase, acid phosphatase, and alkaline phosphatase. *Prog. Biophys. Mol. Biol. 73*, 263–287.
15. Davies, L., Anderson, I. P., Turner, P. C., Shirras, A. D., Rees, H. H., and Rigden, D. J. (2007) An unsuspected ecdysteroid/steroid phosphatase activity in the key T-cell regulator, Sts-1: Surprising relationship to insect ecdysteroid phosphate phosphatase. *Proteins 67*, 720–731.
16. Ogino, T., Matsubara, M., Kato, N., Nakamura, Y., and Mizuno, T. (1998) An *Escherichia coli* protein that exhibits phosphohistidine phosphatase activity towards the HPt domain of the ArcB sensor involved in the multistep His-Asp phosphorelay. *Mol. Microbiol. 27*, 573–585.
17. Mikhailik, A., Ford, B., Keller, J., Chen, Y., Nassar, N., and Carpino, N. (2007) A phosphatase activity of Sts-1 contributes to the suppression of TCR signaling. *Mol. Cell 27*, 486–497.
18. Kleinman, H., Ford, B., Keller, J., Carpino, N., and Nassar, N. (2006) Crystallization and initial crystal characterization of the C-terminal phosphoglycerate mutase homology domain of Sts-1. *Acta Crystallogr. F62*, 218–220.
19. Zhou, X., and Arthur, G. (1992) Improved procedures for the determination of lipid phosphorus by malachite green. *J. Lipid Res. 33*, 1233–1236.
20. Matthews, B. W. (1968) Solvent content of protein crystals. *J. Mol. Biol. 33*, 491–497.
21. Otwinowski, Z., Borek, D., Majewski, W., and Minor, W. (2003) Multiparametric scaling of diffraction intensities. *Acta Crystallogr. A59*, 228–234.
22. Sheldrick, G. M. (2008) A short history of SHELX. *Acta Crystallogr. A64*, 112–122.
23. CCP4 (1994) The CCP4 suite: Programs for protein crystallography, *Acta Crystallogr. D50*, 760−763.
24. Perrakis, A., Sixma, T. K., Wilson, K. S., and Lamzin, V. S. (1997) wARP: improvement and extension of crystallographic phases by weighted averaging of multiple-refined dummy atomic models. *Acta Crystallogr D53*, 448–455.
25. Murshudov, G. N., Vagin, A. A., and Dodson, E. J. (1997) Refinement of macromolecular structures by the maximum-likelihood method. *Acta Crystallogr. D53*, 240–255.
26. Winn, M. D., Isupov, M. N., and Murshudov, G. N. (2001) Use of TLS parameters to model anisotropic displacements in macromolecular refinement. *Acta Crystallogr D57*, 122–133.
27. Laskowski, R. A., Moss, D. S., and Thornton, J. M. (1993) Main-chain bond lengths and bond angles in protein structures. *J. Mol. Biol. 231*, 1049–1067.
28. Morris, G. M., Goodsell, D. S., Halliday, R. S., Huey, R., Hart, W. E., Belew, R. K., and Olson, A. J. (1998) Automated docking using a Lamarckian genetic algorithm and an empirical binding free energy function. *J. Comput. Chem. 19*, 1639–1662.
29. Huey, R., Morris, G. M., Olson, A. J., and Goodsell, D. S. (2007) A semiempirical free energy force field with charge-based desolvation. *J. Comput. Chem. 28*, 1145–1152.
30. Jakalian, A., Jack, D. B., and Bayly, C. I. (2002) Fast, efficient generation of high-quality atomic charges. AM1-BCC model: II. Parameterization and validation. *J. Comput. Chem. 23*, 1623–1641.
31. Pettersen, E. F., Goddard, T. D., Huang, C. C., Couch, G. S., Greenblatt, D. M., Meng, E. C., and Ferrin, T. E. (2004) UCSF Chimera--a visualization system for exploratory research and analysis. *J. Comput. Chem. 25*, 1605–1612.
32. Hamada, K., Kato, M., Shimizu, T., Ihara, K., Mizuno, T., and Hakoshima, T. (2005) Crystal structure of the protein histidine phosphatase SixA in the multistep His-Asp phosphorelay. *Genes Cells 10*, 1–11.
33. Jones, T. A., Zou, J. Y., Cowan, S. W., and Kjeldgaard, M. (1991) Improved methods for building protein models in electron density maps and the location of errors in these models. *Acta Crystallogr. A47* (Part 2), 110–119.
34. Krissinel, E., and Henrick, K. (2007) Inference of macromolecular assemblies from crystalline state. *J. Mol. Biol. 372*, 774–797.
35. Billas, I. M., Iwema, T., Garnier, J. M., Mitschler, A., Rochel, N., and Moras, D. (2003) Structural adaptability in the ligand-binding pocket of the ecdysone hormone receptor. *Nature 426*, 91–96.
36. Jakob, C. G., Lewinski, K., Kuciel, R., Ostrowski, W., and Lebioda, L. (2000) Crystal structure of human prostatic acid phosphatase. *Prostate 42*, 211–218.
37. Kilsheimer, G. S., and Axelrod, B. (1957) Inhibition of prostatic acid phosphatase by alpha-hydroxycarboxylic acids. *J. Biol. Chem. 227*, 879–890.
38. Brunger, A. T. (1993) Assessment of phase accuracy by cross validation: The free R value. Methods and applications. *Acta Crystallogr. D49*, 24–36.
39. Kraulis, P. J. (1991) MOLSCRIPT: A program to produce both detailed and schematic plots of protein structures. *J. Appl. Crystallogr. 24*, 946–950.

BI801318W